A Time-Resolved Resonance Raman Study of Chlorine Dioxide Photochemistry in Water and Acetonitrile

Sophia C. Hayes, Matthew P. Philpott, Steven G. Mayer, and Philip J. Reid*

Department of Chemistry, Box 351700, University of Washington, Seattle, Washington 98195

Received: April 28, 1999

The photochemistry of chlorine dioxide (OClO) in water and acetonitrile is investigated using time-resolved resonance Raman spectroscopy. Stokes and anti-Stokes spectra are measured as a function of time following photoexcitation using degenerate pump and probe wavelengths of 390 nm. For aqueous OClO, the time-dependent Stokes intensities are found to be consistent with the re-formation of ground-state OClO by subpicosecond geminate recombination of the primary ClO and O photofragments. This represents the first unequivocal demonstration of primary-photoproduct geminate recombination in the condensed-phase photochemistry of OClO. Anti-Stokes intensity corresponding to the OClO symmetric stretch is observed demonstrating that, following geminate recombination, excess vibrational energy is deposited along this coordinate. Analysis of the anti-Stokes decay kinetics demonstrates that, in water, intermolecular vibrational relaxation occurs with a time constant of ∼9 ps. For OClO dissolved in acetonitrile, the Stokes scattering intensities are consistent with a significant reduction in the geminate-recombination quantum yield relative to water. Comparison of the OClO anti-Stokes decay kinetics in acetonitrile and water demonstrates that the rate of intermolecular vibrational relaxation is ∼4 times smaller in acetonitrile. Finally, in both solvents the appearance of symmetric-stretch anti-Stokes intensity is significantly delayed relative to geminate recombination. This delay is consistent with the initial deposition of excess vibrational energy along the asymmetric-stretch coordinate followed by intramolecular vibrational energy redistribution. The time scale for this redistribution is ∼5 ps in water and ∼20 ps in acetonitrile suggesting that intramolecular vibrational energy reorganization is solvent dependent.

Introduction

The photochemistry of chlorine dioxide (OClO) has attracted much interest due to its participation in the atmospheric chlorine reservoir as well as its potential role in stratospheric ozone depletion.[1−7] Photoexcitation of OClO results in the production of ClO and O or of Cl and O_2 (Scheme 1).[8−54] In addition, it has been suggested that the formation of Cl occurs through the ground-state decomposition of ClOO formed by photoisomerization of OClO.[2,7,55−60] Current interest in OClO photochemistry involves elucidating the origin of its phase-dependent reactivity. Specifically, the quantum yield for Cl formation (Φ_{Cl}) in the gas phase is ∼0.04 but increases to unity in low-temperature matrixes.[10−12,15−17,39,41,42,45,47,48] The chemistry in solution is intermediate between these two limits with Φ_{Cl} = 0.1−0.2 in water and methanol.[55,56,60−65] Since the environmental impact of OClO arises from its ability to produce atomic chlorine, understanding this phase-dependent reactivity is essential if models capable of predicting the environmental impact of OClO in both homogeneous and heterogeneous settings are to be obtained.

Recent studies of OClO solution-phase photochemistry have attempted to identify the specific solvent−solute interactions that give rise to phase-dependent reactivity of this compound.[53,55,56,60−66] Recently, picosecond and femtosecond pump−probe techniques have been used to monitor the kinetics of photoproduct formation.[55,56,60−65] These studies have provided the first information concerning the dynamics that occur following internal conversion to the ground state. Universal agreement exists concerning the spectral evolution observed in pump−probe studies of aqueous OClO; however, the structural interpretation of this evolution is currently at issue. In the pioneering studies of Simon and co-workers, the spectral evolution was interpreted as being due to the appearance and vibrational relaxation of ground-state ClOO.[55,56,60] In contrast, Keiding and co-workers have suggested that this evolution is more consistent with the appearance of ground-state OClO formed by geminate recombination of the primary ClO and O photofragments.[61−63] Recently, our laboratory has performed pump−probe studies of OClO in water and acetonitrile that demonstrated the spectral evolution observed in acetonitrile is consistent with a 5-fold decrease in the geminate-recombination quantum yield in this solvent relative to water.[64,65] Although these studies have provided insight into the condensed-phase photochemistry of OClO, definitive evidence of the species formed following OClO photoexcitation has yet to be reported. Such information is requisite if differentiation between the current OClO photochemical models is to occur.

SCHEME 1: General Photochemical Pathways Available to OClO following Photoexcitation

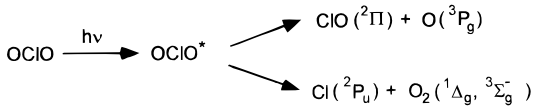

In this manuscript, we present a time-resolved resonance Raman study of OClO dissolved in water and acetonitrile. A

* To whom correspondence should be addressed. E-mail: preid@chem.washington.edu.

10.1021/jp9914065 CCC: $18.00
Published on Web 06/24/1999

preliminary report of this investigation concerning aqueous OClO has appeared.[66] Time-dependent Stokes and anti-Stokes scattering intensities are measured following the photoexcitation of OClO. The temporal evolution in scattered intensity is interpreted with the assistance of computations designed to model the excess-energy dependence of the resonance Raman cross sections. The synergistic application of experimental and computational work presented here provides for three main conclusions regarding the photochemistry of OClO. First, the temporal evolution in OClO Stokes intensity observed in both water and acetonitrile demonstrates that subpicosecond geminate recombination of the primary photofragments occurs resulting in the re-formation of OClO. The geminate recombination quantum yield is determined to be 0.80 ± 0.05 in water, with the efficiency of recombination decreasing by roughly a factor of 5 in acetonitrile. Second, anti-Stokes intensity is observed for transitions corresponding to the symmetric stretch of OClO demonstrating that excess energy is deposited along this coordinate following geminate recombination. The time scale for appearance and decay of anti-Stokes intensity in acetonitrile is significantly longer than in water demonstrating that the vibrational relaxation dynamics are solvent dependent. Third, comparison of the Stokes and anti-Stokes kinetics reveals that, in both solvents, the appearance of symmetric stretch anti-Stokes intensity is delayed relative to geminate recombination. This observation is consistent with the deposition of excess vibrational energy along the asymmetric-stretch coordinate, with the exchange of energy between this coordinate and the symmetric stretch occurring due to intramolecular vibrational energy reorganization.

Experimental Methods

The laser system employed here is identical to that used in our earlier time-resolved work.[64−66] An argon-ion laser (Spectra Physics 2065-07) operating all-lines was used to pump a home-built Ti:sapphire oscillator that produced 30 fs pulses (full-width at half-maximum) centered at 780 nm with a repetition rate of 91 MHz. The oscillator output was temporally elongated using an optical stretcher and delivered to a Ti:sapphire regenerative amplifier (Clark-MXR CPA-1000-PS) equipped with independently tunable single- and double-plate birefringent filters to constrain the amplifier bandwidth. The amplifier output following compression consisted of 500 fs, 700 μJ pulses centered at 780 nm with a spectral width 1.1 times greater than the transform limit (Gaussian pulse shape). The repetition rate of the amplifier was 1 kHz. Frequency doubling of the amplifier output using a 1-mm thick β-BBO crystal (type I) produced both pump and probe beams at 390 nm. The pump beam was temporally advanced or delayed relative to the probe using an optical delay line. The contribution of rotational dynamics to the data was minimized by rotating the polarization of the pump to 54.7° relative to the probe using a zero-order half-wave plate. The instrument response as measured by the optical Kerr effect in water was 700 ± 50 fs.

Time-resolved resonance Raman spectra were obtained as follows. OClO was synthesized as reported elsewhere.[67−69] The pump and probe beams were focused onto a fused-silica flow cell containing ~10 mM solutions of OClO in water (Baker) or acetonitrile (Fisher, spectrophotometric grade) using a 150-mm focal-length, plano-convex, fused-silica lens. A 135° backscattering geometry was employed with the scattered light collected using standard, refractive UV optics and delivered to a 0.5-m focal-length spectrograph (Acton 505F). The spectrograph was equipped with a 1200 grooves/mm classically ruled grating ($\lambda_{blaze} = 500$ nm) for the Stokes experiments or with a 2400 grooves/mm holographic grating for the anti-Stokes experiments. The spectrometer slit widths were adjusted to provide ~15 cm^{-1} resolution. The scattered light was detected by a LN_2-cooled, 1340 × 100 pixel, back-thinned CCD detector (Princeton Instruments). Raman spectra with the "probe-only", the "pump-and-probe", and the "pump-only" incident on the sample were obtained at each time delay. The pump-only spectrum was directly subtracted from the pump-and-probe spectrum to produce the "probe-with-photolysis" spectrum. The probe-only spectrum was then directly subtracted from the probe-with-photolysis spectrum to produce the difference spectra reported here. Six-minute integrations for the Stokes spectra and 10-min integrations for the anti-Stokes spectra were performed for each configuration of the pump and probe at a given delay. Pulse energies were 4 and 0.5 μJ for the pump and probe, respectively. The scattering intensities were found to increase linearly with pump and probe power. Absorption spectra of the sample were obtained before and after an experiment and found to be identical (within experimental error) demonstrating that sample degradation had not occurred during the experiment.

Computational Methods

To assist in interpreting the experimental results presented below, we have computationally investigated the influence of excess vibrational energy on the absorption (σ_A) and resonance Raman cross sections (σ_R) using the time-dependent formalism where the cross sections are given by the following:[70−73]

$$\sigma_A(E_l,T) = \frac{4\pi e^2 E_l M_{eg}^{\ 2}}{6\hbar^2 cn} \sum_i P_i \int_{-\infty}^{\infty} \partial E_{00} H(E_{00}) \int_{-\infty}^{\infty} \langle i|i(t)\rangle \exp[i(E_l + E_i)t/\hbar]\, D(t)\, dt \quad (1)$$

$$\sigma_R(E_l,T) = \frac{8\pi E_s^{\ 3} E_l e^4 M_{eg}^{\ 4}}{9\hbar^6 c^4} \sum_i P_i \int_{-\infty}^{\infty} \partial E_{00} H(E_{00}) \left| \int_0^{\infty} \langle f|i(t)\rangle \exp[i(E_l + E_i)t/\hbar] D(t)\, dt \right|^2 \quad (2)$$

In the above expressions, M_{eg} is the transition moment, E_{00} is the energy difference between the ground- and excited-electronic states, E_l is the energy of the incident radiation, and E_s is the energy of the scattered radiation. $D(t)$ is the homogeneous line width, which is composed of both pure dephasing and population decay. $D(t)$ is modeled as Gaussian consistent with our previous analyses.[67,68] $H(E_{00})$ represents inhomogeneous broadening corresponding to the distribution of E_{00} energies created by different solvent environments that are static on the time scale of Raman scattering. This distribution was modeled as Gaussian with values reported here corresponding to the standard deviation of this distribution. In the evaluation of eqs 1 and 2, it is assumed that the homogeneous and inhomogeneous line widths are independent of excess vibrational energy. The $\langle i|i(t)\rangle$ term in eq 1 represents the time-dependent overlap of the initial state in the absorption process with this same state propagating under the influence of the excited-state Hamiltonian. Similarly, the $\langle f|i(t)\rangle$ term in eq 2 represents the time-dependent overlap of the final state in the Raman-scattering process with the initial state propagating under the influence of the excited-state Hamiltonian. Finally, P_i is the probability of population for a given initial state (see below).

Consistent with our resonance Raman intensity analysis of aqueous OClO,[67] the model for the optically prepared excited-

TABLE 1: $^2A_2$ Excited-State Potential Energy Surface Parameters for OClO in Water[a]

transition[b]	ω_g (cm^{-1})[c]	ω_e (cm^{-1})	Δ[d]
ν_1	945	685	5.63
ν_2	450	284	0.4
ν_3	1100	850	0

[a] Other parameters used to calculate the absorption and Raman cross sections are $\Gamma = 85 \pm 15$ cm^{-1}, inhomogeneous standard deviation = 280 ± 20 cm^{-1}, $M_{eg} = 0.363$ Å, $E_{00} = 18\,900$ cm^{-1}, and $n = 1.35$. [b] Raman transition for which the calculation was performed. The symbols ν_1, ν_2, and ν_3 refer to the symmetric stretch, bend, and asymmetric stretch, respectively. [c] ω_g refers to the ground-state harmonic frequency, and ω_e is the excited-state harmonic frequency. [d] Dimensionless displacement of the excited-state potential energy surface minimum relative to the ground state.

state employed in these calculations was

$$V_e = \frac{1}{2}\frac{(\omega_{e1})^2}{\omega_{g1}}(q_1 - \Delta_1)^2 + \frac{1}{2}\frac{(\omega_{e2})^2}{\omega_{g2}}(q_2 - \Delta_2)^2 + \frac{1}{2}\frac{(\omega_{e3})^2}{\omega_{g3}}(q_3)^2 + \frac{1}{6}\chi_{111}\left(\frac{\omega_{e1}}{\omega_{g1}}\right)^{3/2}(q_1 - \Delta_1)^3 \quad (3)$$

where ω_g and ω_e are the ground- and excited-state frequencies along the symmetric stretch, bend, and asymmetric stretch denoted by the subscripts 1, 2, and 3, respectively. The first three terms in eq 3 represent the harmonic contributions to the potential. Displacement of the excited-state potential-energy-surface minimum relative to the ground state along each coordinate is denoted as Δ, with displacements included for the symmetric coordinates. The term containing χ_{111} is the cubic anharmonicity term involving the symmetric stretch only. The parameters employed in evaluating eqs 1−3 were identical to those determined in the resonance Raman intensity analysis of aqueous OClO.[67] These values are reproduced in Table 1.

Calculation of the time-dependent overlaps ($\langle i|i(t)\rangle$ and $\langle f|i(t)\rangle$) was performed as follows. The ground state was modeled as harmonic, and off-diagonal anharmonicity was not included in the description of the excited state (eq 3); therefore, the multidimensional overlaps can be decomposed into a product of one-dimensional overlaps and calculated independently. The symmetric-stretch overlap was determined using the approximate time-propagator algorithm of Feit and Fleck.[74,75] In this approach, $|i(t)\rangle$ is given by

$$|i(t)\rangle = e^{i(\Delta t)\nabla^2/4M}\, e^{-i(\Delta t)V}\, e^{i(\Delta t)\nabla^2/4M}\, |i(0)\rangle + \vartheta(\Delta t^3) \quad (4)$$

where ∇^2 is the Laplacian in position space, V is the excited-state potential, and Δt is the size of the propagation time step. Time steps of 0.15−0.2 fs were employed with overlaps calculated for times up to 1000 fs. Overlaps involving the bend and asymmetric stretch were determined using the analytic expressions reported by Mukamel and co-workers.[76] The multidimensional absorption or Raman time-dependent overlaps were then obtained by multiplication of the single-mode overlaps.[64,67,68]

Excess-energy dependence of the absorption and Raman cross sections can be ascribed to the energy dependence of the initial-state populations (P_i in eqs 1 and 2). Given this, the excess-energy-dependent absorption and Raman cross sections can be determined by calculating the cross section corresponding to a given initial state and then summing over the manifold of initial states weighed by the probability of occupying these states. Probabilities corresponding to both Boltzmann and non-Boltzmann distributions of excess vibrational energy were investigated. For calculations where this energy is distributed in agreement with Boltzmann statistics, the absorption and Raman cross sections were determined for every ground-state configuration where the total probability (i.e., the product of occupation probabilities for specific levels along each coordinate) was $\geq 1 \times 10^{-5}$. At the highest temperatures investigated, this probability cutoff allowed for the inclusion of >90% of the ground-state population. The cross sections were normalized by dividing the spectrum at a given temperature by the corresponding probability included in the calculation. A decrease in the total-probability cutoff to 1×10^{-6} did not alter the results presented here.

It has been proposed that for OClO, excess-energy deposition and vibrational relaxation involves the asymmetric-stretch coordinate exclusively such that a nonstatistical (or non-Boltzmann) distribution of excess vibrational energy is present following geminate recombination.[62,63] The computational approach employed in this "non-Boltzmann limit" is essentially identical to that described above except that overlaps were calculated by assuming vibrational excitation along the asymmetric stretch only (i.e., $n = 0$ along the symmetric stretch and bend and $n = 0$ to $n = 15$ along the asymmetric stretch). To determine the time-dependent asymmetric-stretch state-occupation probabilities, the vibrational relaxation kinetics were modeled using isolated binary collision (IBC) theory.[77−79] In this model, the vibrational relaxation rate is taken to be linearly dependent on vibrational level:

$$k_{n\rightarrow n-1} = nk_{1\rightarrow 0} \quad (5)$$

where n is the vibrational level and k_{1-0} is the vibrational relaxation rate between $n = 1$ and 0. The simulation of the vibrational-relaxation kinetics was performed as follows. First, OClO was constrained to initially populate $n = 15$ along the asymmetric stretch immediately following recombination since this level is roughly degenerate with the dissociation energy of ground-state OClO ($\sim$17 000 cm^{-1}).[49,51,52,62−64] Coupled differential equations describing the production and decay kinetics for each level along the asymmetric-stretch coordinate were evaluated using eq 5. At various times following recombination, the absorption and Raman cross sections were determined by taking the cross sections corresponding to an individual level along the asymmetric stretch ($\sigma_A(n)$ and $\sigma_R(n)$), multiplying by the probability of populating that level (P_n), and summing over the asymmetric-stretch vibronic manifold as follows:

$$\sigma_A(t) = \sum_{n=0}^{15} \sigma_A(n)P_n(t) \quad (6)$$

$$\sigma_R(t) = \sum_{n=0}^{15} \sigma_R(n)P_n(t) \quad (7)$$

To be consistent with the results of our earlier pump−probe work, k_{1-0} rate constants of 0.07 ps^{-1} in water and 0.015 ps^{-1} in acetonitrile were employed.[64,65] The excess-energy-dependent absorption spectra calculated using the methodology outlined above have been presented previously and are not reproduced here.[64] The interested reader is referred to our earlier work for these results.

Experimental Results

OClO in Water. Figure 1 presents time-resolved Stokes difference spectra of aqueous OClO obtained with pump and probe wavelengths of 390 nm. At 0 ps delay, the difference

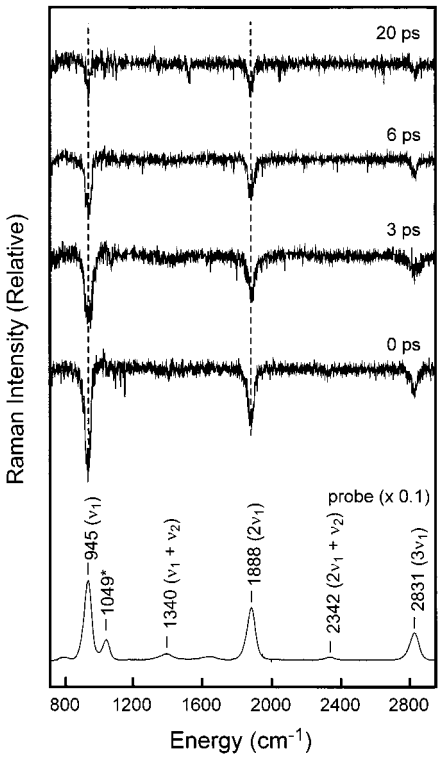

Figure 1. Time-resolved Stokes resonance Raman difference spectra of aqueous OClO. The temporal delay between the pump and probe for a given spectrum is indicated. The probe-only spectrum of aqueous OClO is presented at the bottom of the figure. The transition marked with an asterisk in the probe-only spectrum is due to NO_3^-.

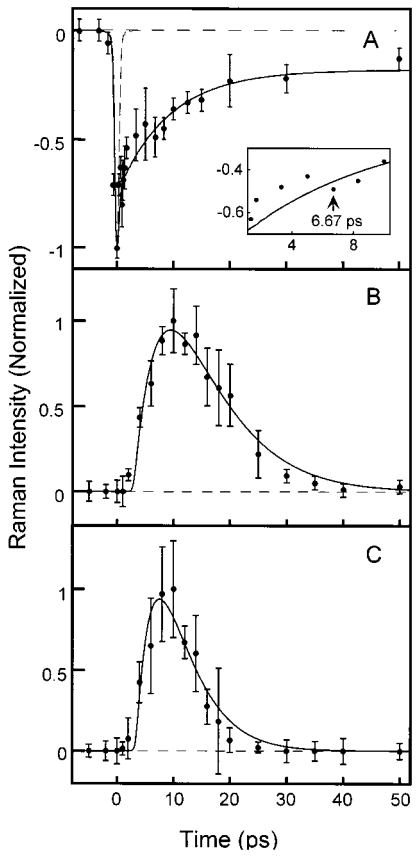

Figure 2. OClO in Water. (A) Intensity of the OClO symmetric stretch fundamental Stokes transition as a function of time. Best fit to the data by a sum of exponentials convolved with the instrument response (solid line) was obtained with time constants (with normalized amplitude in parentheses) of 0.15 ± 0.1 ps (0.65), 9.2 ± 3.5 ps (0.27), and 10 000 ps representing the long-time offset in intensity (0.08). The instrument response (dashed line) is also presented. The insert presents an expanded view of the 2−10 ps region, where a sudden decrease in intensity at ~6 ps is observed. (B) Intensity of the OClO symmetric stretch anti-Stokes fundamental transition as a function of time. Best fit to the data by a sum of two exponentials convolved with the instrument response (solid line) was obtained with an appearance time constant (with normalized amplitude in parentheses) of 5.2 ± 1.5 ps (0.5) and a decay time constant of 9.2 ± 1.7 ps (0.5). (C) Intensity of the OClO symmetric stretch anti-Stokes overtone transition as a function of time. Best fit to the data by a sum of two exponentials convolved with the instrument response (solid line) was obtained with an appearance time constant (with normalized amplitude in parentheses) of 3.3 ± 0.4 ps (0.5) and a decay time constant of 4.4 ± 0.4 ps (0.5).

spectrum demonstrates large, negative intensity (i.e. depletion) for OClO transitions due to photolysis. As the delay between the pump and probe is increased, the extent of this depletion decreases. At 20 ps delay, the depletion is ~20% of the initial amplitude and remains constant out to the longest delays investigated (50 ps). Previous time-resolved resonance Raman studies have demonstrated that time-dependence of the sample optical density can manifest itself as a temporal evolution in scattered intensity.[80] To evaluate the contribution of this effect to the evolution evident in Figure 1, NO_3^- was added to the aqueous sample to serve as a nonphotolabile scattering standard. Figure 1 demonstrates that the NO_3^- transition at 1049 cm^{-1} displays no discernible intensity in the difference spectra at any delay time; therefore, the evolution in sample optical density is not the origin of the intensity evolution.

Kinetic analysis of the data was performed by measuring the integrated intensity of the OClO symmetric-stretch fundamental transition as a function of time (Figure 2A). Comparison of initial depletion amplitude to the depletion that persists at later delays established that the geminate-recombination quantum yield in aqueous solution is 0.80 ± 0.05. This value is in excellent agreement with the results of femtosecond pump−probe studies.[61,64,65] Inspection of Figure 2A demonstrates that recovery of the symmetric-stretch fundamental intensity is biphasic, with roughly 30% of the initial depletion recovering by 1 ps. Consistent with this observation, the data were best modeled by a sum of three exponentials convolved with the instrument response resulting in recovery time constants of 0.15 ± 0.1 ps (i.e., significantly shorter than the instrument-response), 9.2 ± 3.5 ps, and a long-time component (10 000 ps, fixed) representing the persistent depletion in scattering intensity. It is important to note that although the exponential fit to the data reproduces the general intensity evolution, it does not reproduce the more subtle aspects of this evolution. In particular, the insert in Figure 2A provides an expanded view of the depletion intensity between 2 and 10 ps. Deviation between the exponential model and the data is evident with an abrupt decrease in intensity observed at 6 ps. Although modest, the temporal location and extent of this decrease was extremely reproducible between experiments. We will argue below that this evolution is consistent with intravibrational reorganization of excess energy (IVR) occurring on the ~6 ps time scale.

Evidence for the presence of vibrationally excited OClO is provided by the time-resolved anti-Stokes resonance Raman difference spectra presented in Figure 3. At 6 ps, anti-Stokes intensity corresponding to the OClO symmetric-stretch fundamental and overtone transitions is observed at 934 and 1880 cm^{-1}, respectively. The frequencies of these transitions undergo a slight, 6 cm^{-1} increase with delay time consistent with the existence of anharmonicity along the symmetric-stretch

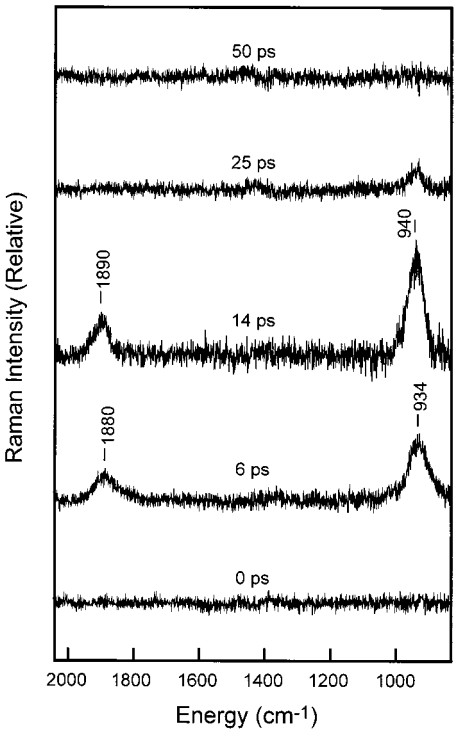

Figure 3. Time-resolved anti-Stokes resonance Raman difference spectra of aqueous OClO. The time delay between the pump and probe for a given spectrum is indicated.

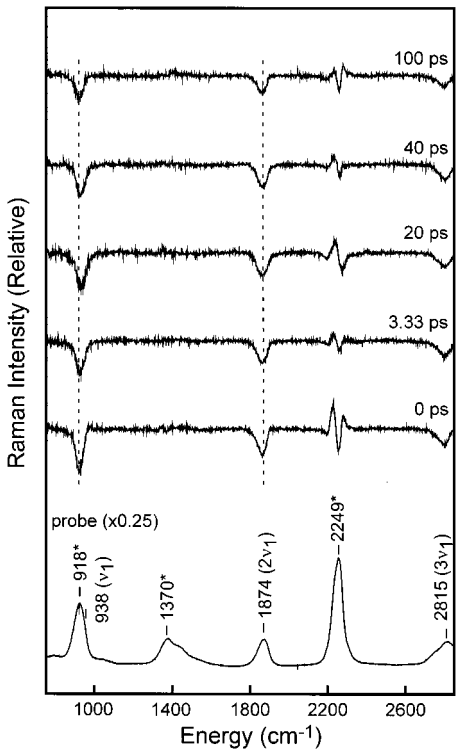

Figure 4. Time-resolved Stokes resonance Raman difference spectra of OClO dissolved in acetonitrile. The time delay between the pump and probe for a given spectrum is presented. The probe-only spectrum of aqueous OClO is also presented. Transitions marked with an asterisk correspond to the solvent.

coordinate.[46,81] Figure 2B,C presents the integrated intensity of the symmetric-stretch fundamental and overtone anti-Stokes transitions, respectively, as a function of time. Best fit to these data by the sum of two exponentials convolved with the instrument response resulted in an appearance time constant for the fundamental of 5.2 ± 1.5 ps and a decay time constant of 9.2 ± 1.7 ps with corresponding time constants of 3.3 ± 0.4 and 4.4 ± 0.4 ps obtained for the overtone. Adequate reproduction of the data required the introduction of a 3 ps delay relative to zero time for the appearance of anti-Stokes intensity for both transitions. We will demonstrate below that this behavior is consistent with initial energy deposition into the asymmetric stretch coordinate followed by IVR.

OClO in Acetonitrile. Figure 4 presents time-resolved resonance Raman difference spectra of OClO in acetonitrile obtained with pump and probe wavelengths of 390 nm. At first appearance, the temporal evolution in scattered intensity observed in this solvent is similar to that in water. The extent of OClO scattering depletion observed at zero time decreases with an increase in delay; however, the extent of depletion at later times is much greater. Consistent with this observation, comparison of the initial depletion to that which persists at later time establishes that the geminate-recombination quantum yield is 0.55 ± 0.05 in acetonitrile. Inspection of the probe-only spectrum in Figure 4 demonstrates that the symmetric-stretch fundamental transition overlaps with the 918 cm^{-1} transition of acetonitrile. To avoid contamination of the kinetics due to the presence of an overlapping solvent transition, we used the symmetric-stretch overtone transition to determine the kinetics of OClO formation in acetonitrile. The possibility exists that the appearance kinetics determined using the overtone transition could differ from those determined using the fundamental transition. To explore this possibility, we determined the kinetics of OClO formation in water using the symmetric-stretch overtone transition (data not shown). The kinetics determined using this transition were identical (within experimental error) to those determined using the fundamental such that the effect of using different Stokes transitions to measure formation kinetics is modest. Figure 5A presents the integrated intensity of the symmetric stretch overtone transition as a function of delay time. Best fit to the data by the sum of three exponentials convolved with the instrument response resulted in a fast recovery time constant of 0.15 ± 0.1 ps (i.e., instrument-response limited), a longer recovery time constant of 33.0 ± 8.1 ps, and a long-time component (10 000 ps, fixed) representing persistent depletion.

The time-resolved resonance Raman anti-Stokes difference spectra of OClO dissolved in acetonitrile are presented in Figure 6. Anti-Stokes intensity corresponding to the symmetric-stretch fundamental and overtone transitions is observed. An increase in the frequency of the symmetric-stretch fundamental transition with increased delay is evident due to anharmonicity along this coordinate. Similar to the behavior seen in the Stokes spectra, the time scale over which OClO anti-Stokes intensity appears and decays is significantly longer in acetonitrile. Specifically, anti-Stokes intensity persists out to 125 ps where the evolution in water is complete by ~30 ps. Figure 5B,C presents the time-dependent anti-Stokes intensity for the symmetric-stretch fundamental and overtone transitions, respectively. Best fit to these data was obtained using a sum of two exponentials convolved with the instrument response resulting in an appearance time constant for the symmetric stretch fundamental transition of 33.7 ± 4.4 ps and a decay time constant of 36.7 ± 4.6 ps. For the symmetric-stretch overtone transition, best fit was accomplished with appearance and decay time constants of 21.4 ± 3.2 and 22.4 ± 3.2 ps, respectively. Similar to water, adequate agreement between the data and fit was accomplished only after the introduction of a ~20 ps delay relative to zero time for both transitions.

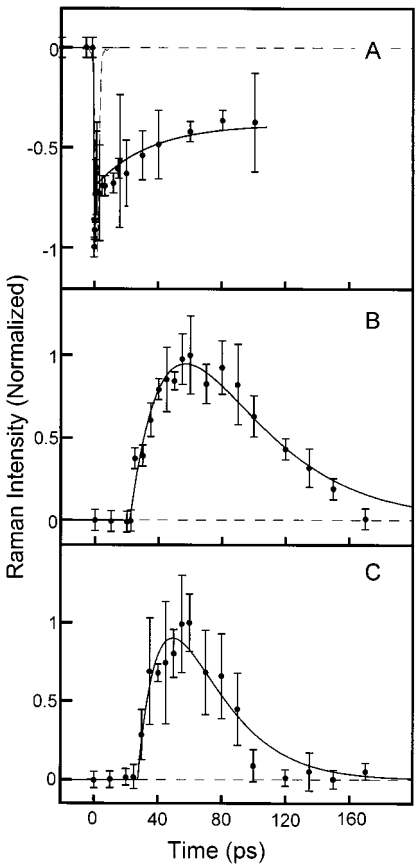

Figure 5. OClO in acetonitrile. (A) Intensity of the OClO symmetric-stretch overtone Stokes transition as a function of time. Best fit to the data by a sum of exponentials convolved with the instrument response (solid line) was obtained with time constants (with normalized amplitude in parentheses) of 0.15 ± 0.1 ps (0.8), 33.0 ± 8.1 ps (0.08), and 10 000 ps representing the long-time offset in intensity (0.12). (B) Intensity of the symmetric stretch anti-Stokes fundamental transition as a function of time. Best fit to the data by a sum of two exponentials convolved with the instrument response (solid line) was obtained with an appearance time constant (with normalized amplitude in parentheses) of 33.7 ± 4.4 ps (0.5) and a decay time constant of 36.7 ± 4.4 ps (0.5). (C) Intensity of the OClO symmetric stretch anti-Stokes overtone transition as a function of time. Best fit to the data by a sum of two exponentials convolved with the instrument response (solid line) was obtained with an appearance time constant (with normalized amplitude in parentheses) of 21.4 ± 3.2 ps (0.5) and a decay time constant of 22.4 ± 3.2 ps (0.5).

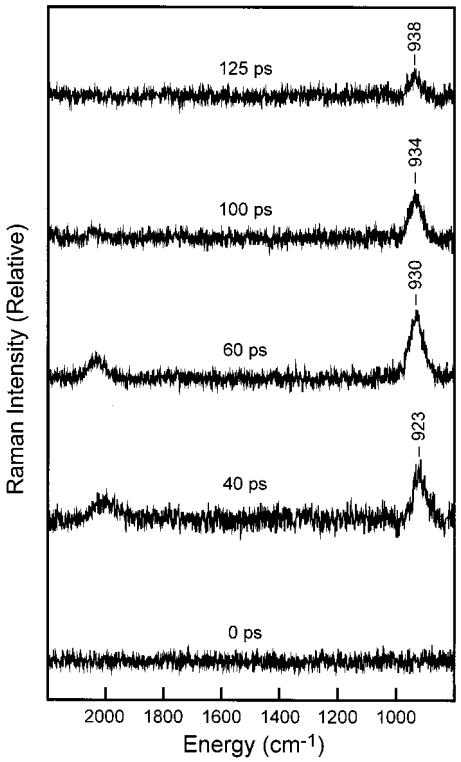

Figure 6. Time-resolved anti-Stokes resonance Raman difference spectra of OClO dissolved in acetonitrile. The time delay between the pump and probe for a given spectrum is indicated.

Computational Results

The temporal evolution in Stokes and anti-Stokes intensities described above can arise from OClO formation via geminate recombination and/or vibrational relaxation. To investigate the influence of excess vibrational energy on the resonance Raman spectra, we have calculated the Stokes and anti-Stokes cross sections as a function of excess vibrational energy. Two energy-deposition limits were considered. First, a Boltzmann distribution of excess vibrational energy was investigated where it was assumed that a statistical distribution of excess energy is established immediately following geminate recombination. Second, a non-Boltzmann distribution of excess vibrational energy was considered where the excess vibrational energy is initially deposited along the asymmetric stretch coordinate and remains along this coordinate during intermolecular vibrational relaxation. The behavior of the Raman cross sections in both limits is presented below.

Boltzmann-Limit Calculations. Figure 7 presents the temperature-dependent Raman Stokes cross sections for the symmetric-stretch fundamental (Figure 7A) and overtone (Figure 7B) transitions. The figure demonstrates that an increase in

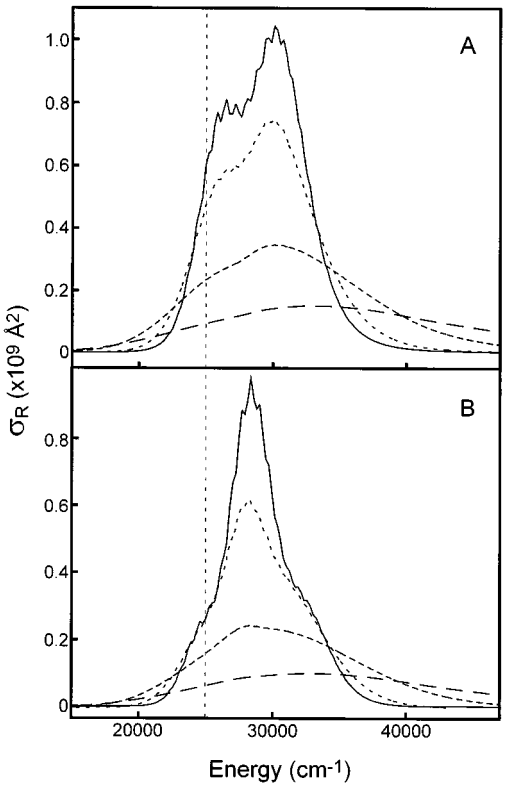

Figure 7. Calculated Raman cross sections for the OClO symmetric stretch fundamental (A) and overtone (B) Stokes transitions as a function of temperature. The curves correspond to molecular temperatures of 298 K (solid), 1000 K (short dash), 3000 K (medium dash), and 7000 K (long dash). The vertical dashed line corresponds to the probe frequency employed in this study.

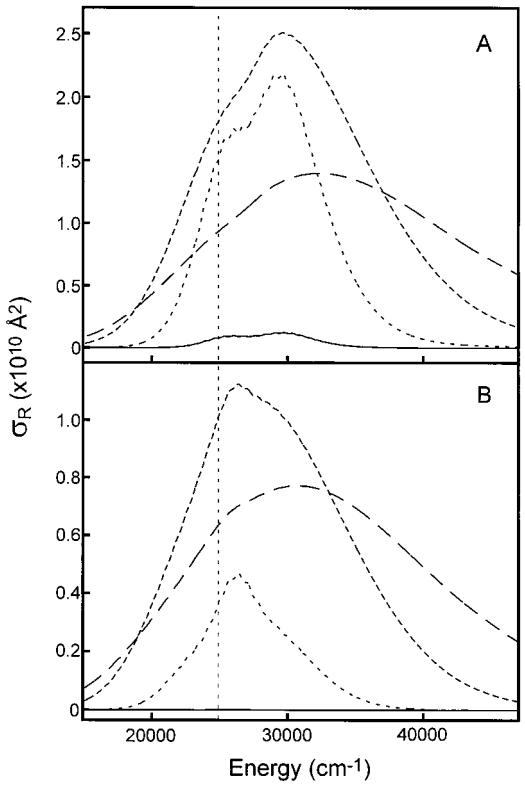

Figure 8. Calculated Raman cross sections for the OClO symmetric stretch fundamental (A) and overtone (B) anti-Stokes transitions as a function of temperature. The curves correspond to molecular temperatures of 298 K (solid), 1000 K (small dash), 3000 K (medium dash), and 7000 K (long dash). The vertical dashed line corresponds to the probe frequency employed in this study.

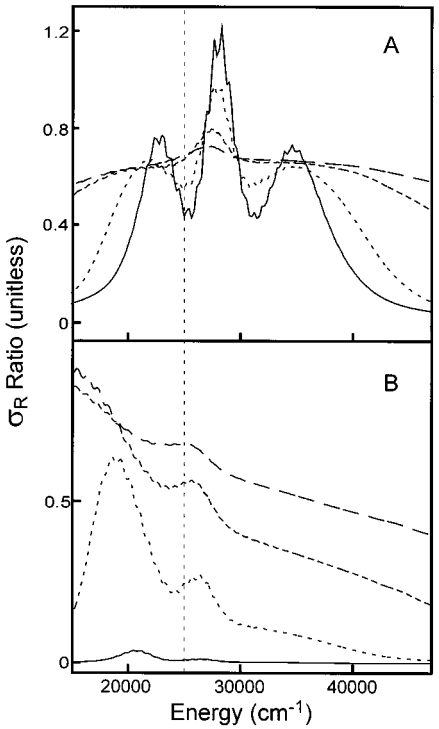

Figure 9. (A) OClO symmetric stretch overtone-to-fundamental Stokes cross section ratio as a function of temperature. (B) OClO symmetric stretch overtone-to-fundamental anti-Stokes cross section ratio as a function of temperature. The curves correspond to molecular temperatures of 298 K (solid), 1000 K (small dash), 3000 K (medium dash), and 7000 K (long dash). The vertical dashed line corresponds to the probe wavelength employed in this study.

temperature is predicted to result in depression of the Raman cross sections and broadening of the excitation profile to higher and lower frequency. The maximum temperature of 7000 K was defined using the heat capacity of OClO combined with the amount of excess vibrational energy available to OClO following recombination ($\sim$17 000 cm^{-1}).[49,51,52,6264] The calculation demonstrates that the observed evolution in scattered intensity due to vibrational relaxation should be extremely probe-wavelength dependent. For example, at 500 nm (20 000 cm^{-1}) the symmetric-stretch fundamental and overtone Stokes cross sections are predicted to increase with temperature; however, opposite behavior is predicted at 390 nm, the probe wavelength employed in this study. Similar behavior has been observed in previous studies of the temperature dependence of absorption and resonance Raman cross sections.[82] The predicted increase in scattering cross section accompanying vibrational relaxation is consistent with the experimental data (Figures 1 and 4). In particular, the $\sim$9 and $\sim$33 ps depletion-recovery times in water and acetonitrile, respectively, are consistent with the recovery in OClO scattering cross section due to vibrational relaxation.

Figure 8A,B presents the calculated temperature-dependent Raman anti-Stokes cross sections for the symmetric-stretch fundamental and overtone transitions, respectively. The temperature dependence observed here is more complicated than that observed for the Stokes cross sections. Specifically, an increase in temperature from 298 to 3000 K is predicted to result in an increase in the anti-Stokes cross sections across the entire excitation profile. However, a further increase in temperature to 7000 K results in a reduction in cross section at the maximum of the excitation profile, with continued increase in the cross sections predicted for frequencies $<$20 000 and $>$40 000 cm^{-1}. Comparison of Figure 8A,B reveals that the temperature dependence of the fundamental and overtone anti-Stokes cross sections is substantially different. Specifically, the overtone cross section is predicted to roughly double between 1000 and 3000 K at 390 nm, but the symmetric stretch is predicted to undergo only a modest increase over this same temperature range. In other words, the intensity of the anti-Stokes overtone transition should decrease more rapidly relative to the fundamental with a reduction in temperature. This prediction is consistent with the anti-Stokes decay kinetics where the overtone decay time constant was significantly smaller than the corresponding time constant for the fundamental transition.

The computational results presented above suggest that a comparison of Stokes or anti-Stokes intensities can be used to determine the temperature of OClO. Figure 9A presents the calculated symmetric-stretch overtone-to-fundamental Stokes cross section ratio as a function of temperature. The figure demonstrates that this ratio is extremely dependent on probe wavelength, and at 390 nm this ratio is expected to be relatively insensitive to temperature. Table 2 presents the experimental ratios obtained in water and acetonitrile. Consistent with the computational prediction, an average intensity ratio of $\sim$0.67 is observed with very little evolution in this value occurring as a function of delay. Figure 9B presents the calculated overtone to fundamental anti-Stokes cross section ratio as a function of temperature. The figure demonstrates that this ratio is predicted to be extremely temperature dependent, and at 390 nm an 8-fold decrease in this ratio should accompany a reduction in temperature from 7000 to 298 K. Table 2 presents the experimental overtone to fundamental anti-Stokes intensity ratio in water and acetonitrile. In water, a significant decrease in this ratio is observed between 6 ps (0.66) and 50 ps (0.08), and an almost identical change is observed in acetonitrile; however, the time scale over which this change occurs is substantially longer.

TABLE 2: Ratios of the Raman Stokes and Anti-Stokes Intensities for the Symmetric Stretch Overtone versus the Fundamental Transition and Corresponding Internal Temperature of OClO

solvent	time (ps)[a]	$\sigma_R^S(2\nu_1)/\sigma_R^S(\nu_1)$[b]	$\sigma_R^{AS}(2\nu_1)/\sigma_R^{AS}(\nu_1)$[c]	est T (K)[d]
water	6.67	0.66	0.66	4500
	10	0.67		
	14	0.67	0.40	1500
	25		0.10	500
	50		0.08	500
acetonitrile	3	0.65		
	20	0.66		
	40	0.70	0.65	4500
	60		0.34	1300
	100	0.70	0.09	500

[a] Pump−probe delay time at which the intensity ratio is obtained. [b] Symmetric-stretch overtone to fundamental Stokes intensity ratio. [c] Symmetric-stretch overtone to fundamental anti-Stokes intensity ratio. [d] Estimated molecular temperature using the computational results presented in Figure 9 and as discussed in the text.

Comparison of the experimental intensity ratios to the computational results presented in Figure 9B results in an estimated molecular temperature of 4500 K at 6 ps in water and 40 ps in acetonitrile and ∼500 K at 50 ps in water and 100 ps in acetonitrile. At this point, it is important to recall that this temperature estimate is made by assuming that a Boltzmann distribution of excess energy exists. Given this assumption, the estimated molecular temperature of 4500 K corresponds to an excess vibrational energy content of ∼9500 cm^{-1}. Since 17 000 cm^{-1} of excess energy is available to OClO following geminate recombination, 7500 cm^{-1} of energy must be lost to the solvent before a statistical distribution of excess vibrational energy is established. In addition, the appearance of anti-Stokes intensity is substantially delayed relative to zero time in both solvents; however, the computational results presented in Figure 8 suggest that even at 7000 K the anti-Stokes cross sections should be appreciable. Therefore, the appearance of anti-Stokes intensity demonstrates excess vibrational energy is eventually deposited along the symmetric stretch; however, this energy must be initially localized along another coordinate where 7500 cm^{-1} of energy is dissipated to the solvent before intramolecular vibrational energy reorganization (IVR) occurs. The behavior of the scattering cross sections before the advent of IVR is considered next.

Non-Boltzmann-Limit Calculations. Recent pump−probe studies of OClO have been interpreted by assuming energy localization along the asymmetric-stretch coordinate.[62,63] To explore this possibility, we have calculated the effect of energy localization along the asymmetric stretch on the Raman cross sections. To accomplish this, we first modeled the vibrational relaxation of OClO using the IBC theory of vibrational relaxation (see above). This formalism is capable of reproducing the majority of the features observed in femtosecond pump−probe studies, and a treatment identical to that presented here was used in our earlier pump−probe work.[64] The results of this analysis for aqueous OClO are presented in Figure 10A where the time-dependent occupation probabilities for levels along the asymmetric stretch coordinate are shown.[64,65] As discussed above, the $n = 15$ level along the asymmetric stretch is expected to be populated immediately after geminate recombination since this level is roughly degenerate with the 17 000 cm^{-1} of excess energy available to OClO following recombination. The figure demonstrates that as time increases, population cascades down the asymmetric-stretch vibrational-state manifold. Using the occupation probabilities presented in Figure 10A to ascertain

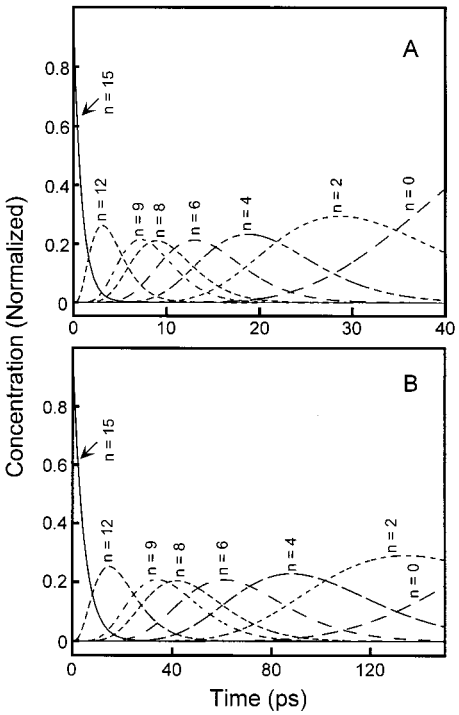

Figure 10. Temporal profiles of the population of individual levels along the asymmetric stretch as a function of time. Excess vibrational energy after geminated recombination is deposited along the asymmetric stretch, and the molecule vibrationally relaxes according to IBC model presented in the text. (A) Calculation for water employing a k_{1-0} rate constant of 0.07 ps^{-1}. (B) Calculation for acetonitrile employing a k_{1-0} rate constant of 0.015 ps^{-1}. Rate constants employed are those obtained from the analysis of our earlier pump−probe work.[64,65]

the time-dependent energy content of OClO, we find that a residual energy of 9500 cm^{-1} (the amount of energy determined to exist after IVR given the Boltzmann-limit analysis presented above) is established 6 ps after geminate recombination. This is exactly the time where nonexponential evolution in the Stokes scattering intensities is observed, and is markedly similar to the 3 ps delay observed for the appearance in anti-Stokes intensity. Figure 10B presents the corresponding IBC calculation for OClO in acetonitrile. Here, the reduction in the k_{1-0} rate results in a reduction in overall relaxation rate down the asymmetric-stretch manifold. It is important to note that the maximum OClO temperatures found in water and acetonitrile (see above) are equivalent, suggesting that a similar amount of energy is lost to the solvent before IVR. Using the probabilities presented in Figure 10B, a residual energy of 9500 cm^{-1} is achieved at ∼25 ps following geminate recombination. This is entirely consistent with the ∼20 ps delay in the appearance of anti-Stokes intensity along the symmetric stretch.

If the nonexponential evolution in Stokes scattering observed in water (insert in Figure 2A) is due to IVR, the Stokes cross sections must be different between the non-Boltzmann and Boltzmann limits at a similar internal energy. Figure 11 presents the dependence of the symmetric-stretch Stokes fundamental and overtone cross sections on population of individual levels along the asymmetric stretch ($n = 0$ to $n = 15$). The figure demonstrates that as higher levels along the asymmetric stretch are populated, the symmetric stretch Stokes cross sections are reduced. In addition, the excitation profile broadens slightly and shifts to lower energy. The Stokes cross sections are reduced with an increase in energy along the asymmetric-stretch coordinate, reminiscent of the behavior observed in the Boltzmann limit; however, the extent of this reduction is different.

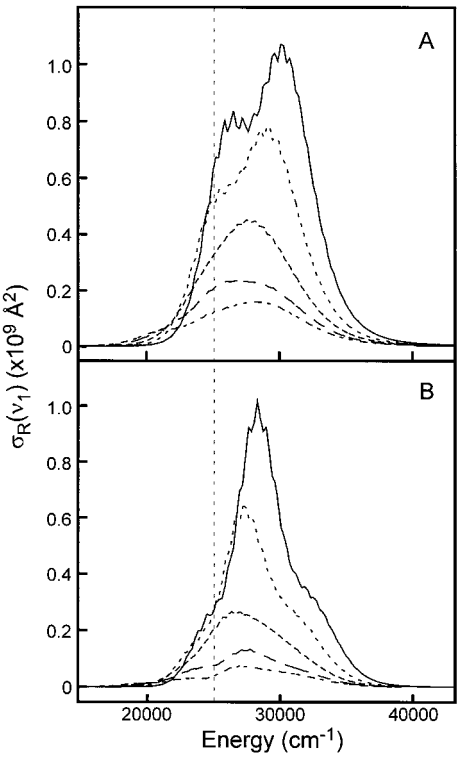

Figure 11. Raman cross sections for the OClO symmetric stretch fundamental (A) and overtone (B) Stokes transitions as a function of excess vibrational energy localized along the asymmetric stretch. The curves correspond to population of $n = 0$ (solid), 4 (short dashed), 8 (medium dashed), 12 (long dashed), and 15 (dot dashed) vibrational levels along the asymmetric stretch coordinate. The vertical dashed line corresponds to the probe frequency employed in this study.

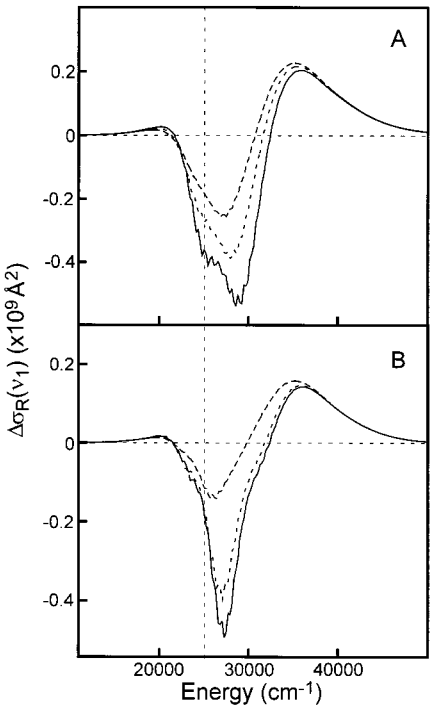

Figure 12. Difference in Raman cross sections for the symmetric stretch fundamental (A) and overtone (B) Stokes transitions between the non-Boltzmann and Boltzmann relation limits. The curves correspond to the difference between the calculated Raman cross sections with $n = 4$ (solid), 6 (short dashed), and 8 (medium dashed) and the calculated Raman cross section at 4500 K. The vertical dashed line represents the probe wavelength employed in this study.

Figure 12A,B presents the difference between the Stokes cross sections calculated in the non-Boltzmann and Boltzmann limits for the symmetric-stretch fundamental and overtone transitions, respectively. The figure depicts the difference in cross section between the non-Boltzmann limit with population of $n = 4$, 6, and 8 along the asymmetric stretch (considered since these levels are populated to the greatest extent at 6 ps) versus the Boltzmann limit cross sections at a temperature of 4500 K. The figure demonstrates that, at 390 nm, IVR is expected to be evidenced by a reduction in Stokes intensity for both the symmetric-stretch fundamental and overtone transitions, consistent with the sudden increase in depletion intensity observed in water at ~6 ps (Figure 2A).

Discussion

Geminate Recombination. The subpicosecond recovery in Stokes intensity following the photoexcitation of OClO provides an unequivocal demonstration that geminate recombination of the primary photofragments results in the re-formation of ground-state OClO. The subpicosecond recombination dynamics observed here are similar to the rates observed in other systems. In the classic work of Harris and co-workers on the photodissociation dynamics of I_2, it was demonstrated that geminate recombination of the I fragments occurs in <2 ps.[78] Recent femtosecond pump−probe studies of I_2^- photodissociation by Barbara and co-workers have demonstrated that geminate recombination of the photofragments occurs on the subpicosecond time scale.[83] Most salient to the studies presented here, pump−probe studies on the photodissociation of the polyatomic species methylene iodide (CH_2I_2) in a variety of solvents demonstrated that geminate recombination of the primary photofragments occurs in 350 fs.[84] Given the rapidity of these dynamics, it was concluded that recombination occurred after a single collision with the solvent (i.e., diffusional processes do not participate in the recombination). In addition, the recombination kinetics were found to be independent of solvent suggesting that the structural details of the surrounding solvent shell were of minor importance in defining the rate of recombination. The rapid geminate-recombination dynamics observed for OClO in both water and acetonitrile demonstrate that primary recombination dominates over slower diffusional-dependent recombination. In addition, the similarity in recombination kinetics between water and acetonitrile suggests that the structural details of the solvent are not primarily responsible for defining the recombination rate. However, it should be noted that the geminate recombination dynamics are dependent on actinic pulse energy, with the extent of geminate recombination decreasing with an increase in actinic energy.[63] In addition, earlier pump−probe work employing photoexcitation at 355 nm assigned dynamics occurring on the subnanosecond time scale to diffusional processes.[56] Therefore, the extent of solvent dependence demonstrated by the geminate-recombination dynamics may depend on the energy content of the photofragments.

Although the rate of geminate recombination is similar in both water and acetonitrile, the extent of geminate recombination is dependent on solvent. Specifically, the larger residual depletion in Stokes scattering intensity observed in acetonitrile relative to water (Figures 5A and 2A, respectively) is consistent with a substantial reduction in the geminate-recombination quantum yield in acetonitrile. This observation supports the results of earlier pump−probe studies where an increase in a long-time depletion in optical density at probe wavelengths resonant with the ground-state absorption band of OClO was observed in

acetonitrile relative to water and attributed to a decrease in the geminate-recombination quantum yield.[64] Solvent dependence of geminate recombination quantum yields has also been observed in the photodissociation of I_2^- with the quantum yield decreasing from 0.93 in water to 0.68 in acetonitrile and acetone.[83] It was suggested that intermolecular hydrogen bonding present in polar, protic solvents (such as water) stabilizes the surrounding solvent shell providing for more efficient trapping of the photofragments. In polar-aprotic solvents, the absence of intermolecular hydrogen bonds would make the first solvent shell more labile to photofragment cage escape. The results presented here support this hypothesis.

Vibrational Relaxation Dynamics. *Intramolecular Vibrational Reorganization (IVR).* The time-resolved resonance Raman data provide information concerning the time scale for intramolecular vibrational energy reorganization (IVR). Most research in this area has focused on systems in the gas phase where the intramolecular interactions responsible for energy reorganization can be studied in the absence of solvent-mediated processes.[85−87] In the majority of these studies, an optically active or "bright" state is populated, and the dynamics of energy flow from the bright state into other states (so-called "dark states") is monitored. The experiments presented here can be described within this conceptual framework. Assuming that OClO is initially produced with excess vibrational energy localized along the asymmetric stretch, the experiments presented here can be viewed as a conventional IVR experiment where the prepared state is optically dark and population of the optically bright symmetric stretch via IVR is monitored.[88]

The Stokes and anti-Stokes data presented above provide a detailed picture of the IVR dynamics. One of the most interesting results presented above is that the subpicosecond recovery of symmetric-stretch Stokes intensity is not reflected by a similar, rapid appearance of anti-Stokes intensity. Although this effect could be due to small anti-Stokes cross sections at the probe wavelength employed, the computational results presented above demonstrate that the anti-Stokes scattering cross sections should be appreciable. Therefore, the discrepancy between the rapid OClO Stokes recovery kinetics and the slower appearance of symmetric stretch anti-Stokes intensity suggests that geminate recombination of the ClO and O fragments results in the production of OClO that is vibrationally cold along the symmetric stretch. This conclusion is entirely consistent with femtosecond pump−probe studies of aqueous OClO that have been interpreted in terms of geminate recombination resulting in energy deposition along the asymmetric-stretch coordinate exclusively.[62,63] The nonexponential evolution of the Stokes intensities in water provides additional evidence that IVR is delayed relative to geminate recombination. Specifically, the Stokes data demonstrate a discrete increase in depleted intensity at ∼6 ps (inset of Figures 1 and 4). Comparison of the calculated symmetric stretch fundamental and overtone cross sections in the non-Boltzmann and Boltzmann limits demonstrates that the onset of IVR should be evidenced by a decrease in scattering intensity (Figure 12), a prediction consistent with the intensity change seen in H_2O. In acetonitrile, nonexponential evolution in the Stokes data is difficult to observe due to the reduced efficiency of geminate recombination. However, a substantial delay in symmetric-stretch anti-Stokes intensity is observed relative to geminate recombination suggesting that IVR occurs ∼20 ps following geminate recombination in this solvent. Given these observations, we conclude that immediately following geminate recombination, OClO is produced with excess vibrational energy deposited along the asymmetric-stretch coordinate. The IBC description of the vibrational relaxation combined with the molecular temperature estimates provided by the anti-Stokes intensities demonstrates that roughly ∼7500 cm^{-1} of excess energy is deposited into the solvent during the initial relaxation involving the asymmetric stretch. Following this initial relaxation, IVR occurs with a time constant of ∼5 ps in water and ∼20 ps in acetonitrile.

The vibrational relaxation dynamics of OClO provide insight into the interplay between energy dissipation to the solvent and IVR. Solution phase vibrational relaxation studies have been dominated by diatomic systems in which IVR is not operative.[78,79,83,89−99] Triatomic systems such as OClO represent the simplest class of molecules in which the effect of intermolecular energy dissipation on IVR can be studied. Perhaps the most intriguing discovery to emerge from the results presented above is that the time scale for energy deposition into the symmetric-stretch coordinate is solvent dependent. In addition, the similarity in maximum solute temperature determined through analysis of the anti-Stokes intensities suggests that the similar levels of the asymmetric-stretch vibronic manifold must be reached before IVR takes place. One possible explanation for this behavior is that, at early times, the high degree of OClO excitation results in the predominance of a local-mode description of the coordinates favoring energy localization into a single Cl−O bond. With energy dissipation, a transition from local to normal coordinates occurs promoting IVR. The bifurcation of normal modes at high excitation energies and the effect of bifurcation on intramolecular energy flow including the generation of energy "bottlenecks" has been recognized.[100,101] Further studies of the vibrational relaxation dynamics of OClO including monitoring the energy content of the asymmetric stretch with visible-pump/infrared-probe techniques should provide further information concerning the dynamics and solvent dependence of IVR.

Intermolecular Vibrational Relaxation. The results presented here demonstrate that the intermolecular vibrational relaxation dynamics of OClO are solvent dependent. Specifically, the agreement between later-time recovery in Stokes intensity and the decay time of the anti-Stokes intensity demonstrates that intermolecular relaxation occurs with a ∼9 ps time constant in water and a ∼35 ps time constant in acetonitrile. Although we can conclude that the OClO−solvent interactions must be substantially different between water and acetonitrile for a 4-fold change in the vibrational-relaxation rate to exist, the question remains as to what interactions are responsible for this difference.

Studies of vibrational relaxation have shown that two energy-dissipation mechanisms dominate in solution: vibrational to translational (V−T) and vibrational to vibrational (V−V) energy transfer.[79,102] Furthermore, it has been suggested that at high vibrational levels V−T relaxation is most efficient, but V−V transfer dominates at lower levels. This turnover in dissipation mechanisms is reflected by recent studies of Stratt and coworkers where short-time solvent−solute dynamics were found to be dominated by collisional-type interactions of the solute with a single solvent molecule or two.[95] In addition, this collisional-type interaction was found to be solvent independent where the longer-time dynamics did demonstrate solvent dependence. With application of this conceptual framework to OClO, the solvent dependence of intermolecular vibrational relaxation suggests that intermolecular energy dissipation is dominated by V−V relaxation. Assuming that V−V energy transfer dominates the later-time relaxation dynamics, the increased vibrational-relaxation rate in water relative to acetonitrile can be viewed as an increase in resonance between solvent

and solute modes participating in the relaxation process. The effect of solvent friction on intermolecular vibrational relaxation has been of much recent interest, and the dependence of intermolecular vibrational relaxation on solvent friction is evident in the expression for the single-model relaxation rate:[78,83,90,92,94−97,103−112]

$$k_{\nu\rightarrow\nu'} = \frac{g(\omega_{\nu'\nu})^2}{\hbar^2} |\langle\nu|Q|\nu'\rangle|^2 \left\{1 + \coth\left(\frac{\hbar\omega_{\nu'\nu}}{2kT}\right)\right\} \mathrm{Im}\chi(\omega_{\nu'\nu}) \quad (8)$$

where $k_{\nu\rightarrow\nu'}$ represents the state-to-state relaxation rate constant, $g(\omega)$ is the solvent−solute coupling strength, and the solvent friction is contained in Im(χ) (the imaginary part of the Raman susceptibility). The frequency dependence of Im(χ) can be measured through optically heterodyned optical Kerr effect measurements for low frequencies and depolarized Raman data for higher frequencies as recently demonstrated by Castner and co-workers for water.[113−115] Equation 8 demonstrates that the rate of vibrational relaxation is dependent on the solvent−solute coupling strength as well as the frequency-dependent solvent friction. What remains to be established is which solvent-frequency components are operative in the vibrational-relaxation dynamics of OClO.

Typically, low-frequency solute modes dominate intermolecular relaxation since the density of solvent accepting modes is greatest for these modes.[77] For OClO, the lowest frequency coordinate is the bend at 450 cm^{-1}. The frequency overlap between this mode and the librational modes of water is excellent;[115] however, the librational modes of acetonitrile are located at lower frequency ($\sim$100 cm^{-1}) such that the overlap with the bend is poor.[116,117] If we consider the symmetric- (938 cm^{-1}) and asymmetric-stretch (1100 cm^{-1}) coordinates of OClO, these transitions are well matched to the symmetric stretch (918 cm^{-1}) and methyl-rock (1124 cm^{-1}) modes of acetonitrile such that appreciable friction should be experienced by these coordinates, but the friction in water should be less. Since that the vibrational relaxation rate is greater in water, the above comparisons suggest that the V−V relaxation dynamics are dominated by coupling between the bend and the solvent. Clearly, monitoring the vibrational energy content of the bend should prove quite interesting. In addition, comparison of the vibrational relaxation dynamics in two polar-aprotic solvents having different frequency-dependent susceptibilities should also be very informative concerning the importance of V−V transfer processes involving higher-frequency coordinates.

Intermolecular hydrogen bonding could also be responsible for solvent dependence of intermolecular vibrational relaxation. Various studies have suggested that solvent−solute hydrogen bonding can dramatically alter the time scale for vibrational relaxation.[118−120] In studies by Hochstrasser and co-workers, the vibrational relaxation times observed for N_3^- in D_2O, H_2O, and methanol were significantly shorter than in the aprotic solvent hexamethylphosphoramide (HMPA) demonstrating the importance of intermolecular hydrogen bonding as a pathway for energy dissipation.[118] The authors also found a correlation between solute mode-frequency shifts in the various solvents and the rate of vibrational relaxation, with an increase in solute vibrational frequency correlating with an increase in the relaxation rate. The symmetric stretch of OClO shifts in frequency from 945 cm^{-1} in water to 938 cm^{-1} in acetonitrile consistent with this correlation. In studies by Sastry et al., an increase in the line width of the acetonitrile CN-stretch transition was observed with the addition of water implying that an increase in the vibrational-relaxation rate occurs due to solvent−solute hydrogen bonding.[120] Finally, Chen and Schwartz have investigated the effects of hydrogen bonding on the vibrational relaxation dynamics of halomethanes by analyzing the isotropic Raman line widths of CD_2Br_2 and $CHBr_3$ in various solvents.[119] The authors observed a dramatic decrease in vibrational relaxation time in hydrogen-bonding solvents as evidenced by an increase in the Raman line width.

Long-range electrostatic effects represent a final potential source for the increase in the OClO vibrational relaxation rate in water relative to acetonitrile. It has been demonstrated that the coupling of solute-charge evolution to solvent relaxation can be an efficient mechanism for energy deposition into the solvent.[83,90,92,94] For example, studies by Hochstrasser and co-workers have demonstrated that, for CN^- dissolved in water, the vibrational relaxation rate correlates with the infrared absorption cross section of the solvent implying that Coulombic interactions are operative in promoting vibrational relaxation.[92] In addition, theoretical and experimental studies comparing the relaxation of I_2^- to I_2 have demonstrated that the change in solute-charge distribution during relaxation causes an acceleration of energy dissipation to the solvent.[83,94] Coulombic effects are expected to be of minimal importance in OClO since this compound is neutral. However, OClO is an open-shell system such that solvent induced radical localization could represent a potential mechanism for solvent−solute coupling. This mechanism can be viewed as being similar to the solvent-dependent charge localization dynamics observed for I_3^-. In this system, the presence of asymmetric-stretch fundamental resonance Raman intensity was observed indicating that the solvent promotes charge localization on one end of the molecule.[121] In OClO, fundamental intensity involving the asymmetric stretch coordinate has not been observed in solution to date; therefore, the existence of solvent-induced radical localization is speculative at best.[67,68]

Other Photoproducts. The Stokes difference spectra presented in Figures 1 and 4 demonstrate that the photochemical dynamics observed at this probe wavelength are dominated by geminate recombination. However, other photochemical processes may also be important. For example, the photoisomerization of OClO to form the peroxy isomer, ClOO, has been postulated to occur in solution.[55,56,60] This hypothesis is entirely reasonable given that photoisomerization resulting in the formation ClOO dominates the photochemical behavior of OClO trapped in low-temperature matrixes.[38−40,42−48] Low-temperature matrix infrared absorption studies have assigned transitions at 373, 407, and 1441 cm^{-1} to ClOO.[47] The difference spectra presented in Figures 1 and 4 demonstrate no noticeable intensity at $\sim$1400 cm^{-1}. Furthermore, although the $<$500 cm^{-1} region was not studied, overtone intensity corresponding to either low-frequency mode of ClOO was not observed. Similar arguments apply to $ClClO_2$.[40] It should be noted that optical density increases in the UV observed in pump−probe studies of OClO are consistent with ClOO and/or $ClClO_2$ formation.[61−65,122] Time-resolved resonance Raman experiments performed with a probe wavelength of 260 nm are currently underway to ascertain the existence of ClOO or $ClClO_2$.[123]

Given the results presented here, it appears that the photoproduct formation dynamics are significantly different in solution relative to low-temperature matrixes. We suggest two potential explanations for this difference in reactivity. First, resonance Raman intensity analysis studies of OClO have demonstrated that the excited-state reaction dynamics are extremely dependent on solvent;[67,68,81] therefore, the excited-state reactivity of OClO may be different in solution relative to

matrixes. Second, ClOO and $ClClO_2$ are labile to thermal decomposition and/or further thermal reactivity. For example, the barrier for the ground-state isomerization of ClOO to OClO has been estimated to be only 0.67 kcal/mol ($\sim$230 cm^{-1}).[57] Given this small energy barrier, we might expect that the photochemical production of ClOO to be followed by rapid isomerization to form OClO given the elevated molecular temperatures achieved following internal conversion (see above). In short, the efficient caging of molecular fragments combined with the low temperatures at which matrix-isolation work is performed presumably results in the stabilization of species that are not stable under the conditions at which the solution-phase experiments are performed.

Conclusions

In this manuscript, we have presented an investigation of the geminate recombination and vibrational-relaxation dynamics of OClO in water and acetonitrile using time-resolved resonance Raman spectroscopy. The subpicosecond recovery in OClO Stokes depletion provides an unequivocal demonstration that the re-formation of OClO via geminate recombination occurs in solution. This subpicosecond geminate recombination was observed in both water and acetonitrile demonstrating that the dynamics of geminate recombination are not dependent on solvent. However, the larger residual depletion in scattered intensity evident at longer delays in acetonitrile relative to water demonstrates that the geminate-recombination quantum yield is solvent dependent. Time-resolved anti-Stokes spectra demonstrate that excess vibrational energy is deposited into the asymmetric stretch coordinate following geminate recombination. Dissipation of this energy to the solvent occurs with a time constant of $\sim$9 ps in water and $\sim$36 ps in acetonitrile. A delay in the appearance of OClO anti-Stokes intensity relative to geminate recombination is observed in both water and acetonitrile consistent with initial deposition of the excess vibrational energy into the asymmetric-stretch coordinate. Analysis of the Stokes and anti-Stokes intensities indicated that intramolecular vibrational redistribution of the excess vibrational energy occurs with a time constant of $\sim$5 ps in water and $\sim$20 ps in acetonitrile. In summary, the results presented here provide a detailed description of the geminate recombination and vibrational relaxation dynamics of OClO. The information presented here provides greater insight into the reaction dynamics of OClO and should prove useful in understanding the ground-state reactivity of this compound.

Acknowledgment. The National Science Foundation is acknowledged for their support of this work through the CAREER program (Grant CHE-9701717). Acknowledgment is also made to the donors of the Petroleum Research Fund, administered by the American Chemical Society. P.J.R. is a recipient of a Camille and Henry Dreyfus New Faculty Award and is a Cottrell Fellow of the Research Corp. We also acknowledge useful conversations with Richard Stratt (Brown U.) concerning his recent work.

References and Notes

(1) Pfeilsticker, K.; Blom, C. E.; Brandtjen, R.; Fischer, H.; Glatthor, N.; Grendel, A.; Gulde, T.; Hopfner, M.; Perner, D.; Piesch, C.; Platt, U.; Renger, W.; Sessler, J.; Wirth, M. *J. Geophys. Res.* **1997**, *102*, 10801.
(2) Vaida, V.; Simon, J. D. *Science* **1995**, *268*, 1443.
(3) Sessler, J.; Chipperfield, M. P.; Pyle, J. A.; Toumi, R. *Geophys. Res. Lett.* **1995**, *22*, 687.
(4) Burkholder, J. B.; Talukdar, R. K.; Ravishankara, A. R. *Geophys. Res. Lett.* **1994**, *21*, 585.
(5) Rowland, F. S. *Annu. Rev. Phys. Chem.* **1991**, *42*, 731.
(6) Solomon, S.; Sanders, R. W.; Miller Jr., H. L. *J. Geophys. Res.* **1990**, *95*, 13807.
(7) Vaida, V.; Solomon, S.; Richard, E. C.; Ruhl, E.; Jefferson, A. *Nature* **1989**, *342*, 405.
(8) Richard, E. C.; Vaida, V. *J. Chem. Phys.* **1991**, *94*, 153.
(9) Richard, E. C.; Vaida, V. *J. Chem. Phys.* **1991**, *94*, 163.
(10) Bishenden, E.; Donaldson, D. J. *J. Chem. Phys.* **1994**, *101*, 9565.
(11) Bishenden, E.; Donaldson, D. J. *J. Chem. Phys.* **1993**, *99*, 3129.
(12) Bishenden, E.; Haddock, J.; Donaldson, D. J. *J. Phys. Chem.* **1991**, *95*, 2113.
(13) Delmdahl, R. F.; Baumgartel, S.; Gericke, K.-H. *J. Chem. Phys.* **1996**, *194*, 2883.
(14) Baumert, T.; Herek, J. L.; Zewail, A. H. *J. Chem. Phys.* **1993**, *99*, 4430.
(15) Davis, H. F.; Lee, Y. T. *J. Chem. Phys.* **1996**, *105*, 8142.
(16) Davis, H. F.; Lee, Y. T. *J. Phys. Chem.* **1992**, *96*, 5681.
(17) Lawrence, W. G.; Clemitshaw, K. C.; Apkarian, V. A. *J. Geophys. Res.* **1990**, *95*, 18591.
(18) Flesch, R.; Wassermann, B.; Rothmund, B.; Ruhl, E. *J. Phys. Chem.* **1994**, *98*, 6263.
(19) Marston, G.; Walker, I. C.; Mason, N. J.; Gingell, J. M.; Zhao, H.; Brown, K. L.; Motte-Tollet, F.; Delwiche, J.; Siggel, M. R. F. *J. Phys. B: At. Mol. Opt. Phys.* **1998**, *31*, 3387.
(20) Gulley, R. J.; Field, T. A.; Steer, W. A.; Mason, N. J.; Lunt, S. L.; Ziesel, J.-P.; Field, D. *J. Phys. B: At. Mol. Opt. Phys.* **1998**, *31*.
(21) Ludowise, P.; Blackwell, M.; Chen, Y. *Chem. Phys. Lett.* **1997**, *273*, 211.
(22) Lin, J. J.; Hwang, D. W.; Lee, Y. T.; Yang, X. *J. Chem. Phys.* **1998**, *108*, 10061.
(23) Roth, M.; Maul, C.; Gericke, K. H. *J. Chem. Phys.* **1997**, *107*, 10582.
(24) Furlan, A.; Scheld, H. A.; Huber, J. R. *J. Chem. Phys.* **1997**, *106*, 6538.
(25) Ruehl, E.; Jefferson, A.; Vaida, V. *J. Phys. Chem.* **1990**, *94*, 2990.
(26) Tanaka, K.; Tanaka, T. *J. Mol. Spectrosc.* **1983**, *98*, 425.
(27) Hamada, Y.; Merer, A. J.; Michielsen, S.; Rice, S. A. *J. Mol. Spectrosc.* **1981**, *86*, 4995.
(28) Michielsen, S.; Meyer, A. J.; Rice, S. A.; Novak, F. A.; Freed, K. F.; Hamada, Y. *J. Chem. Phys.* **1981**, *74*, 3089.
(29) McDonald, P. A.; Innes, K. K. *Chem. Phys. Lett.* **1978**, *59*, 562.
(30) Curl, R. F.; Abe, K.; Bissinger, J.; Bennett, C.; Tittel, F. K. *J. Mol. Spectrosc.* **1973**, *48*, 72.
(31) Krishna Pillai, M. G.; Curl, R. F. *J. Chem. Phys.* **1962**, *37*, 2921.
(32) Sakurai, K.; Clark, J.; Broida, H. P. *J. Chem. Phys.* **1971**, *54*, 1217.
(33) Brand, J. C. D.; Redding, R. W.; Richardson, A. W. *J. Mol. Spectrosc.* **1970**, *34*, 399.
(34) Coon, J. B. *J. Chem. Phys.* **1946**, *14*, 665.
(35) Coon, J. B. *Phys. Rev.* **1940**, *58*, 926.
(36) Lai, L.-H.; Liu, C.-P.; Lee, Y.-P. *J. Chem. Phys.* **1998**, *109*, 988.
(37) Liu, C.-P.; Lai, L.-H.; Lee, Y.-Y.; Hung, S.-C.; Lee, Y.-P. *J. Chem. Phys.* **1998**, *109*, 978.
(38) Graham, J. D.; Roberts, J. T.; Brown, L. A.; Vaida, V. *J. Phys. Chem.* **1996**, *100*, 3115. Brown, L. A.; Vaida, V.; Hanson, D. R.; Graham, J. D.; Roberts, J. T. *J. Phys. Chem.* **1996**, *100*, 3121.
(39) Graham, J. D.; Roberts, J. T.; Anderson, L. D.; Grassian, V. H. *J. Phys. Chem.* **1996**, *100*, 19551.
(40) Gane, M. P.; Williams, N. A.; Sodeau, J. R. *J. Chem. Soc., Faraday Trans.* **1997**, *93*, 2747.
(41) Lanzendorf, E. J.; Kummel, A. C. *Geophys. Res. Lett.* **1996**, *23*, 1251.
(42) Pursell, C. J.; Conyers, J.; Alapat, P.; Parveen, R. *J. Phys. Chem.* **1995**, *99*, 10433.
(43) Mueller, H. S. P.; Willner, H. *J. Phys. Chem.* **1993**, *97*, 10589.
(44) Johnsson, K.; Engdahl, A.; Ouis, P.; Nelander, B. *J. Mol. Struct.* **1993**, *293*, 137.
(45) Adrian, F. J.; Bohandy, J.; Kim, B. F. *J. Chem. Phys.* **1986**, *85*, 2692.
(46) Chi, F. K.; Andrews, L. *J. Mol. Spectrosc.* **1974**, *52*, 82.
(47) Arkell, A.; Schwager, I. *J. Am. Chem. Soc.* **1967**, *89*, 5999.
(48) Rochkind, M. M.; Pimentel, G. C. *J. Chem. Phys.* **1967**, *46*, 4481.
(49) Gole, J. L. *J. Phys. Chem.* **1980**, *84*, 1333.
(50) Peterson, K. A. *J. Chem. Phys.* **1998**, *109*, 8864.
(51) Peterson, K. A.; Werner, H.-J. *J. Chem. Phys.* **1996**, *105*, 9823.
(52) Peterson, K. A.; Werner, H.-J. *J. Chem. Phys.* **1992**, *96*, 89481.
(53) Brusa, M. A.; Perissinotti, L. J.; Churio, M. S.; Colussi, A. J. *J. Photochem. Photobiol. A, Chem.* **1996**, *101*, 105.
(54) Churio, M. S.; Brusa, M. A.; Perissinotti, L. J.; Ghibaudi, E.; Coronel, M. E. J.; Colussi, A. J. *Chem. Phys. Lett.* **1995**, *232*, 237.
(55) Chang, Y. J.; Simon, J. D. *J. Phys. Chem.* **1996**, *100*, 6406.
(56) Dunn, R. C.; Flanders, B. N.; Simon, J. D. *J. Phys. Chem.* **1995**, *99*, 7360.
(57) Vaida, V.; Goudjil, K.; Simon, J. D.; Flanders, B. N. *J. Mol. Liq.* **1994**, *61*, 133.

(58) Dunn, R. C.; Simon, J. D. *J. Am. Chem. Soc.* **1992**, *114*, 4856.
(59) Dunn, R. C.; Flanders, B. N.; Vaida, V.; Simon, J. D. *Spectrochim. Acta* **1992**, *48A*, 1293.
(60) Dunn, R. C.; Richard, E. C.; Vaida, V.; Simon, J. D. *J. Phys. Chem.* **1991**, *95*, 6060−6063.
(61) Thøgersen, J.; Jepsen, P. U.; Thomsen, C. L.; Poulsen, J. A.; Byberg, J. R.; Keiding, S. R. *J. Phys. Chem. A* **1997**, *101*, 3317.
(62) Poulsen, J. A.; Thomsen, C. L.; Keiding, S. R.; Thøgersen, J. *J. Chem. Phys.* **1998**, *108*, 8461.
(63) Thøgersen, J.; Thomsen, C. L.; Poulsen, J. A.; Keiding, S. R. *J. Phys. Chem. A* **1998**, *102*, 4186.
(64) Philpott, M. J.; Hayes, S. C.; Reid, P. J. *Chem. Phys.* **1998**, *236*, 207.
(65) Philpott, M. J.; Charalambous, S.; Reid, P. J. *Chem. Phys. Lett.* **1997**, *281*, 1.
(66) Hayes, S. C.; Philpott, M. J.; Reid, P. J. *J. Chem. Phys.* **1998**, *109*, 2596.
(67) Foster, C. E.; Reid, P. J. *J. Phys. Chem. A* **1998**, *102*, 3541.
(68) Esposito, A.; Foster, C.; Beckman, R.; Reid, P. J. *J. Phys. Chem. A* **1997**, *101*, 5309.
(69) Reid, P. J.; Esposito, A. P.; Foster, C. E.; Beckman, R. A. *J. Chem. Phys.* **1997**, *107*, 8262.
(70) Myers, A. B. *J. Raman Spectrosc.* **1997**, *28*, 389.
(71) Myers, A. B. *Chem. Phys.* **1994**, *180*, 215.
(72) Myers, A. B.; Li, B. *J. Chem. Phys.* **1990**, *92*, 3310.
(73) Lee, S.-Y.; Heller, E. J. *J. Chem. Phys.* **1979**, *71*, 4777.
(74) Feit, M. D.; Fleck, J. A. *J. Chem. Phys.* **1983**, *78*, 301.
(75) Feit, M. D.; Fleck, J. A.; Steiger, A. *J. Comput. Phys.* **1982**, *47*, 412.
(76) Sue, J.; Mukamel, S. *J. Chem. Phys.* **1987**, *88*, 651.
(77) Oxtoby, D. W. *Adv. Chem. Phys.* **1981**, *47*, 487.
(78) Harris, A. L.; Brown, J. K.; Harris, C. B. *Annu. Rev. Phys. Chem.* **1988**, *39*, 341.
(79) Nesbitt, D. J.; Hynes, J. T. *J. Chem. Phys.* **1982**, *77*, 2130.
(80) Reid, P. J.; Lawless, M. K.; Wickham, S. D.; Mathies, R. A. *J. Phys. Chem.* **1994**, *98*, 5597.
(81) Esposito, A. P.; Stedl, T.; Jonsson, H.; Reid, P. J.; Peterson, K. A. *J. Phys. Chem. A* **1999**, *103*, 1748.
(82) Shreve, A. P.; Mathies, R. A. *J. Phys. Chem.* **1995**, *99*, 7285.
(83) Walhout, P. K.; Alfano, J. C.; Thakur, K. A. M.; Barbara, P. F. *J. Phys. Chem* **1995**, *99*, 7568.
(84) Schwartz, B. J.; King, J. C.; Harris, C. B. *The Molecular Basis of Solvent Caging*; Simon, J. D., Ed.; Kluwer: Dordrecht, The Netherlands, 1994.
(85) Gruebele, M.; Bigwood, R. *Int. Rev. Phys. Chem.* **1998**, *17*, 91.
(86) Nesbitt, D. J.; Field, R. W. *J. Phys. Chem.* **1996**, *100*, 12735.
(87) Boyall, D.; Reid, K. L. *Chem. Soc. Rev.* **1997**, *26*, 223.
(88) Since the asymmetric stretch is nontotally symmetric in the C_{2v} point group of ground-state OClO, fundamental resonance Raman intensity is not allowed on the basis of symmetry.
(89) Van Der Zwan, G.; Hynes, J. T. *Physica A* **1983**, *121A*, 227.
(90) Whitnell, R. M.; Wilson, K. R.; Hynes, J. T. *J. Phys. Chem.* **1990**, *94*, 8625.
(91) Heilweil, E. J.; Doany, F. E.; Moore, R.; Hochstrasser, R. M. *J. Chem. Phys.* **1982**, *76*, 5632.
(92) Hamm, P.; Lim, M.; Hochstrasser, R. M. *J. Chem. Phys.* **1997**, *107*, 10523.
(93) Barbara, P. F.; Walker, G. C.; Smith, T. P. *Science* **1992**, 975.
(94) Benjamin, I.; Whitnell, R. M. *Chem. Phys. Lett.* **1993**, *204*, 45.
(95) Ladanyi, B. M.; Stratt, R. M. *J. Phys. Chem. A* **1998**, *102*, 1068.
(96) Larsen, R. E.; Stratt, R. M. *J. Chem. Phys.* **1999**, *110*, 1036.
(97) Benjamin, I.; Barbara, P. F.; Gertner, B. J.; Hynes, J. T. *J. Phys. Chem.* **1995**, *99*, 7557.
(98) Lingle, R.; Xu, X.; Yu, S.-C.; Zhu, H.; Hopkins, J. B. *J. Chem. Phys.* **1990**, *93*, 5667.
(99) Xu, X.; Lingle, R.; Yu, S.-C.; Chang, Y. J.; Hopkins, J. B. *J. Chem. Phys.* **1990**, *92*, 2106.
(100) Lu, Z.-M.; Kellman, M. E. *Chem. Phys. Lett.* **1995**, *247*, 195.
(101) Kellman, M. E.; Chen, G. *J. Chem. Phys.* **1991**, *95*, 8671.
(102) Xu, X.; Yu, S.-C.; Lingle, R.; Zhu, H.; Hopkins, J. B. *J. Chem. Phys.* **1991**, *95*, 2445.
(103) Walhout, P. K.; Silva, C.; Barbara, P. F. *J. Phys. Chem.* **1996**, *100*, 5188.
(104) Kliner, D. A. V.; Alfano, J. C.; Barbara, P. F. *J. Chem. Phys.* **1993**, *98*, 5375.
(105) Whitnell, R. M.; Wilson, K. R.; Hynes, J. T. *J. Chem. Phys.* **1992**, *96*, 5354.
(106) Rey, R.; Hynes, J. T. *J. Chem. Phys.* **1998**, *108*, 142.
(107) Hofmann, M.; Graener, H. *Chem. Phys.* **1996**, *206*, 129.
(108) Gnanakaran, S.; Hochstrasser, R. M. *J. Chem. Phys.* **1996**, *105*, 3486.
(109) Pugliano, N.; Szarka, A. Z.; Gnanakaran, S.; Triechel, M.; Hochstrasser, R. M. *J. Chem. Phys.* **1995**, *103*, 6498.
(110) Owrutsky, J. C.; Raftery, D.; Hochstrasser, R. M. *Annu. Rev. Phys. Chem.* **1994**, *45*, 519.
(111) Pugliano, N.; Palit, D. K.; Szarka, A. Z.; Hochstrasser, R. M. *J. Chem. Phys.* **1993**, *99*, 7273.
(112) Kuehne, T.; Voehringer, P. *J. Chem. Phys.* **1996**, *105*, 10788.
(113) Castner, E. W.; Maroncelli, M. *J. Mol. Liq.* **1998**, *77*, 1.
(114) Cho, M.; J., R. S.; Scherer, N. F.; Ziegler, L. D.; Fleming, G. R. *J. Chem. Phys.* **1992**, *96*, 5033.
(115) Castner, E. W.; Chang, Y. J.; Chu, Y. C.; Walrafen, G. E. *J. Chem. Phys.* **1995**, *102*, 653.
(116) McMorrow, D.; Lotshaw, W. T. *J. Phys. Chem.* **1991**, *95*, 5.
(117) Chang, Y. J.; Castner, E. W. *J. Chem. Phys.* **1993**, *99*, 113.
(118) Li, M.; Owrutsky, J.; Sarisky, M.; Culver, J. P.; Yodh, A.; Hochstrasser, R. M. *J. Chem. Phys.* **1993**, *98*, 5499.
(119) Chen, A. F. T.; Schwartz, M. *Spectrochim. Acta A* **1987**, *43A*, 1151.
(120) Sastry, M. I. S.; Singh, S. *Curr. Sci.* **1986**, *55*, 1157.
(121) Johnson, A. E.; Myers, A. B. *J. Chem. Phys.* **1995**, *102*, 3519.
(122) Mauldin, R. L., III; Burkholder, J. B.; Ravishankara, A. R. *J. Phys. Chem.* **1992**, *96*, 2582.
(123) Philpott, M. J.; Hayes, S. C.; Reid, P. J. *J. Phys. Chem. A*, manuscript in preparation.